PCCP

PAPER

View Article Online
View Journal

Cite this: DOI: 10.1039/c9cp00093c

The correlation between electrical conductivity and second-order Raman modes of laser-reduced graphene oxide†

Bing Ma, Raul D. Rodriguez,* Alexey Ruban, Sergey Pavlov and Evgeniya Sheremet

Raman spectroscopy is the tool of choice in the physicochemical investigation of carbon nanomaterials. However, Raman analysis of graphene oxide (GO) is lagging in comparison to the rich information gained in the case of carbon nanotubes and graphene. Here, we carried out a joint current sensing atomic force microscopy (CSAFM) and Raman spectroscopy investigation of laser-reduced GO. Reduced graphene oxide (rGO) was obtained under different laser powers in the range from 0.1 to 10 mW (532 nm). We compare the Raman spectra and the electrical conductivity at the nanoscale obtained by current sensing atomic force microscopy. Our analysis shows that three bands in the second-order region (2D, D + G, 2G), in the range from 2500 to 3200 cm^{-1}, are uniquely sensitive to the degree of reduction. Moreover, we found that the changes in peak area ratios A_{D+G}/A_D and A_{2G}/A_D show a direct correlation with the electrical resistance of rGO. We establish an optical micro-spectroscopy way to assess the degree of reduction in laser-reduced GO. These new insights provide a convenient and useful way to investigate the reduction of rGO from the fitting analysis of Raman spectra, becoming a useful tool in fundamental research and the development of rGO-based microdevices.

Received 7th January 2019,
Accepted 24th April 2019

DOI: 10.1039/c9cp00093c

rsc.li/pccp

Introduction

Graphene, a two-dimensional (2D) sheet of sp^2-hybridized carbon,[1] has fuelled the interest of the scientific community especially considering that it has been intensively investigated since 2004.[2] This interest is mainly due to graphene's unique and useful properties: mechanical and chemical stability, high electron mobility, and optical transparency.[3–5] These properties have made possible the development of several graphene-based devices with ultra-high performance such as transistors and sensors.[6,7] In this sense, graphene oxide (GO), the oxidized form of graphene, has also attracted the interest of the community working on these novel 2D materials. This interest in GO is because this material has several advantages over graphene such as easy and inexpensive production and water solubility which favors solution-processing fabrication methods. One of the most significant benefits that rGO has over graphene is the possibility to easily control the electrical conductivity, hydrophilicity, and degree of transparency by tuning its level of oxidation.[8] Several methods can be used to tune the level of oxidation, such as chemical reagent reduction, thermal annealing, laser annealing, *etc.*[9] Chemical reduction, using different chemical reagents such as hydrazine, sodium borohydride, or vitamin C, is an easily available way to obtain reduced graphene oxide (rGO). This method can produce large quantities of rGO, but it may involve other functional groups from reducing agents like nitrogen groups.[9–11] Upon thermal annealing, GO decomposes into graphene-like rGO, CO and CO_2 gases originating from the oxygen-containing groups between the GO sheets. Meanwhile, thermal annealing removes carbon atoms from the GO layer since it creates CO and CO_2 gases, which split the graphene sheets into smaller pieces giving way to additional distortion of the sp^2 carbon plane. Hence, this method is good in producing small sized but wrinkled graphene sheets due to the gas production during reduction.[9,12,13] The transformation of GO to rGO by laser annealing is an efficient, easy-to-make, and environmentally friendly method to obtain a graphene-like material on arbitrary substrates, and even on temperature sensitive polymers.[14,15] The lower environmental impact of laser reduction is thanks to the lower energy necessary for laser operation in contrast to the thermal annealing in an oven that has a considerably larger energy consumption. Furthermore, laser annealing can produce GO with arbitrary geometries (patterning) to fabricate, for example, microelectronic circuits.[16] In this regard, laser annealing appears to be a popular and versatile way to achieve rGO. By controlling the laser irradiation

Tomsk Polytechnic University, Lenina ave. 30, 634034, Tomsk, Russia.
E-mail: rodriguez@tpu.ru

† Electronic supplementary information (ESI) available. See DOI: 10.1039/c9cp00093c

parameters, like power and exposure time, we can obtain rGO with different degrees of reduction. Moreover, the irradiation wavelength used in the laser-reduction of GO can be used to highlight thermal and photochemical contributions.[17] Therefore, finding a convenient way to analyze the degree of reduction of rGO is of wide interest to many scientific groups, providing critical information for device applications such as electrical conductivity.

Raman spectroscopy is the tool of choice in the analysis of carbon nanomaterials.[18,19] A large number of studies are continuously being reported focusing on the application of Raman spectroscopy to analyze graphene and its derivatives.[20] Moreover, in recent work reported by Claramunt *et al.* they investigated how to use Raman spectroscopy to analyze the degree of reduction of rGO based on two additional bands D* and D″ between 1100 and 1800 cm^{-1}.[21] They focused on the D* band (between 1150 and 1200 cm^{-1}) assigned to a disordered graphitic lattice provided by sp^2–sp^3 bonds at the edges of carbon networks.[22] They also reported the D″ band (between 1500 and 1550 cm^{-1}) related to the phonon density of states in finite-size crystals of graphite[23] or an amorphous lattice.[24] The critical point in Claramunt's work is that the authors concluded that the D* and D″ positions could be correlated with the oxygen content of rGO obtained by thermal annealing. However, when we reproduced their analysis on laser-reduced rGO samples, we found that their method gave very high uncertainties for the peak positions due to a high convolution upon fitting the peaks between the D and G bands. Therefore, we aimed at finding an alternative way to correlate the degree of reduction of rGO with the Raman spectra. This investigation was largely driven by our practical need to assess how much GO is actually reduced. Motivated by this, we performed a systematic study on laser-reduced rGO by Raman and conductive AFM. GO was reduced using a laser with different powers (from 0.1 mW to 10 mW) which resulted in rGO with different levels of reduction. The direct correlation between the resistance and the parameters of a particular set of Raman bands is discussed here showing that Raman spectroscopy can be used for the electrical conductivity evaluation of laser-reduced GO.

Experimental

Materials

Graphene oxide water dispersion (4 mg ml^{-1}, water) was commercially available from "Graphenea", Spain. The single-layer character of GO was verified for highly diluted solutions deposited on glass and analyzed by atomic force microscopy showing GO flakes with a lateral size of several micrometers and *ca.* 1 nm single-layer thickness. The original GO concentration 4 mg ml^{-1} was diluted 20 times in ultra-pure water. This GO dispersion was used to obtain a 103 nm thick GO film as described below.

Sample preparation

The substrate used as a support for the GO films consists of an Au-coated 10 × 13 mm glass prepared by thermal evaporation of an Au film 100 nm in an ultra-high vacuum. We chose this Au-coated substrate to obtain the electrical conductivity of the rGO structures in parallel to Raman spectroscopy analysis. Before depositing GO, the substrate was cleaned by rinsing with acetone, ethanol, and ultra-pure water, respectively. After drying, 0.2 ml diluted GO was deposited on the substrate and allowed to dry under room conditions. The deposited GO on Au resulted in a uniform film (*ca.* 103 nm thick) which was reduced by using a tightly-focused laser beam from the Raman equipment (532 nm, 50× objective and lens with N.A. 0.5). Different laser powers of 0.1 mW, 0.5 mW, 1 mW, 2 mW, 4 mW, 6 mW, 8 mW, and 10 mW were measured using an internal power meter providing an estimation of the laser power on the surface of the sample. These illumination conditions resulted in reduced GO spots with a diameter of 1.3 μm obtained under laser power densities (on the surface of the sample) of 0.75×10^8, 3.77×10^8, 7.53×10^8, 1.51×10^9, 3.01×10^9, 4.52×10^9, 6.03×10^9, 7.53×10^9 W m^{-2}. The irradiation time for all powers was 0.2 s. The reduced patterns resulted in circular spots with a diameter of about 1.3 μm as shown in Fig. 1.

Raman experiments

At room temperature, rGO spot-patterned samples were obtained and analyzed *in situ* using a DXR2xi Raman Imaging Microscope (Thermo Fisher Scientific USA). Raman experiments were performed under laser excitation at 532 nm wavelength (100× objective and lens N.A. 0.9). To minimize the modifications of the rGO films, we chose a laser power of 0.1 mW for all Raman spectroscopy experiments reported here (0.1 mW was the lowest laser power allowed by the instrument). These irradiation conditions resulted in a laser beam spot with 0.72 μm diameter and a power density of 2.46×10^8 W m^{-2} on the sample surface.

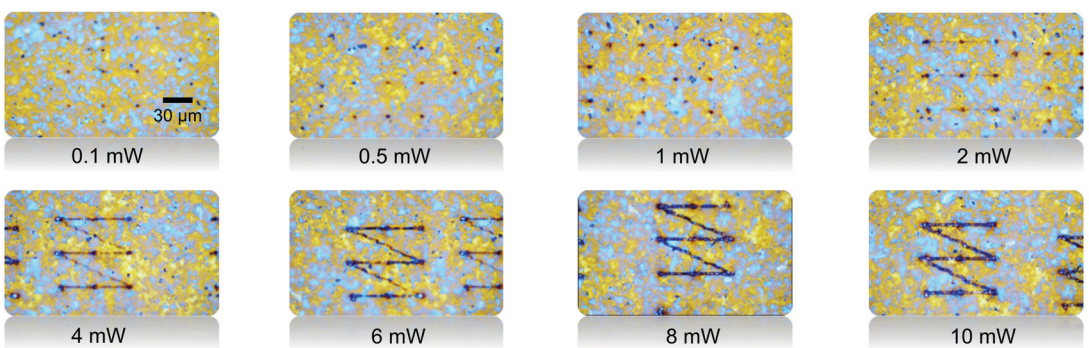

Fig. 1 Optical micrographs of the rGO laser-irradiated 3 × 3 arrays obtained under different laser powers.

It is worth noting in time-dependent studies (data are shown in Fig. S1, ESI†) that after GO was reduced, this minimum laser power of 0.1 mW did not induce any additional changes. For each rGO area obtained at different laser powers, the Raman laser was focused at the center of the rGO spot with a 100× objective. Each rGO spot was then measured with an exposure time of 1 s and 10 repetitions to obtain statically-averaged spectra. A Voigt function was used to fit the peaks in the range from 1000 to 1800 cm^{-1} while a Lorentzian function was used to fit the peaks in the second-order range from 2500 to 3300 cm^{-1}. The bands in the range from 1000 to 1800 cm^{-1} were fitted by 6 peaks which were assigned to D*, D, D″, G, D′, and M. The bands in the range from 2500 to 3200 cm^{-1} were fitted by 3 peaks which were assigned to 2D, D + G, and 2G. The fitting parameters of all peaks like FWHMs, areas, and positions were collected and analyzed.

Current-sensing atomic force microscopy (CSAFM) experiments

The current images and *I–V* curves for different rGO samples were obtained using an NTEGRA scanning probe microscope (NTMDT, Russia). The scanning speed was about 15 μm s^{-1}. The bias voltage used for the acquisition of current images was 0.5 V. After acquiring a current image, several *I–V* curves were recorded and averaged over each region of interest for different laser irradiated rGO spots. The *I–V* curves of rGO were used to calculate the averaged resistance for each spot. The CSAFM investigation showed a uniform current distribution in the laser-irradiated spots. This relative uniformity is evidenced in the histogram of the current values shown in Fig. S3b (ESI†); the histogram obtained from the current image shows a sharp peak at 0 nA originating from the non-conductive GO, and a broader peak around 24 nA originating from the rGO conductivity.

Results and discussion

Optical microscopy images

The optical microscopy images of our samples are shown in Fig. 1. The laser-induced rGO patterns in our work are 3 × 3 spot arrays shown in Fig. 1. Except for the black points that are mostly from rGO, the rest of the sample is GO as confirmed by the Raman hyperspectral imaging of the sample shown in Fig. S1 (ESI†). The different color contrasts in yellow and blue are due to optical interference due to changes in thickness. In Fig. 1, we can see the color of the points becoming darker as the laser power increases. This observation is in agreement with previous reports.[25,26] In those articles, the authors also showed that with further reduction the rGO became darker. Here, when the laser power increases to 2 mW, we see the lines between the points becoming more visible. These lines occur because when the laser power increases to 2 mW, it is large enough that the GO sample gets reduced as the laser spot moves from one point to another under constant illumination. This result illustrates the high sensitivity of GO to laser irradiation, emphasizing that during the Raman analysis, GO can be further reduced. Taking this into account, we notice that previous reports on the Raman analysis of GO using high laser power densities could have induced the unintentional modification of GO by the Raman laser itself.[27]

CSAFM analysis

CSAFM was performed to obtain the resistance of the rGO regions from *I–V* curves. This method is particularly beneficial in our case since otherwise, it would have been extremely challenging to contact the sample to evaluate its conductivity electrically. Spectroscopic methods such as X-ray photoelectron spectroscopy (XPS), X-ray diffraction, and thermogravimetric analysis are used to evaluate the C/O ratio degree. However, the laser-reduced graphene oxide spots in our work have spatial dimensions in the range of 3 μm, which are beyond the spatial resolutions of XPS or other methods, except for CSAFM. This is the reason why we exploited CSAFM as a measure of reduction reflected by the local conductivity of the sample at the nano-scale. Fig. 2b shows the CSAFM *I–V* curves of GO and rGO reduced using a laser with a power of 8 mW. In Fig. 2b we can see that rGO is conductive while GO is not. Note also the decrease in the slope of the current which is not due to the properties of rGO, but is observed when reaching the nonlinear response range of the nanoamperometer. A hysteresis of about 0.6 mV in the *I–V* curves is a negligible value that is not much higher than the instrumental error (±0.25 mV). This hysteresis could also be affected by the nonlinear response of the nanoamperometer, and therefore we do not discuss it further here. According to the *I–V* curves, we calculated the resistance values of rGO areas obtained under different laser powers. In Fig. 2c, we see that the rGO resistance decreases with increasing laser power. We should notice that even the lowest laser power of 0.1 mW is large enough to reduce GO as can be seen from the Raman map in the ESI,† Fig. S1. Moreover, the power dissipated in the films during local resistivity measurements due to current flow was estimated to be in the order of nano-Watts using the equation $P = I \times V$, where we considered I = 20 nA and V = 0.5 V. This Joule heating is negligible compared to the laser power in the order of milli-Watts used for GO reduction. Additional reduction during the Raman experiment was also ruled out. This is possible by observing that once GO was reduced, the 0.1 mW laser power did not induce further changes in the rGO regions. This is evidenced from the optical image of the laser-reduced pattern that retains its color after a Raman map was performed at 0.1 mW (Fig. S1b, ESI†). This optical contrast is contrary to the changes in the GO film that becomes darkened due to the laser reduction during Raman imaging at 0.1 mW. As we mentioned before, the resistance of rGO is related to the degree of reduction, with higher reduction, the electrical resistance of rGO decreases. We find it more convenient to use a $\log_{10}$-scale instead of a linear scale to represent more clearly this power dependency. The linear-scale plot of resistance *vs.* laser power is shown in the ESI,† Fig. S2. The resistance of rGO appears to be relatively large due to the small area of the CSAFM tip (a circular contact in the order of 50 nm radius). We can make a rough estimate for the electrical conductivity of the rGO pattern by considering it as a

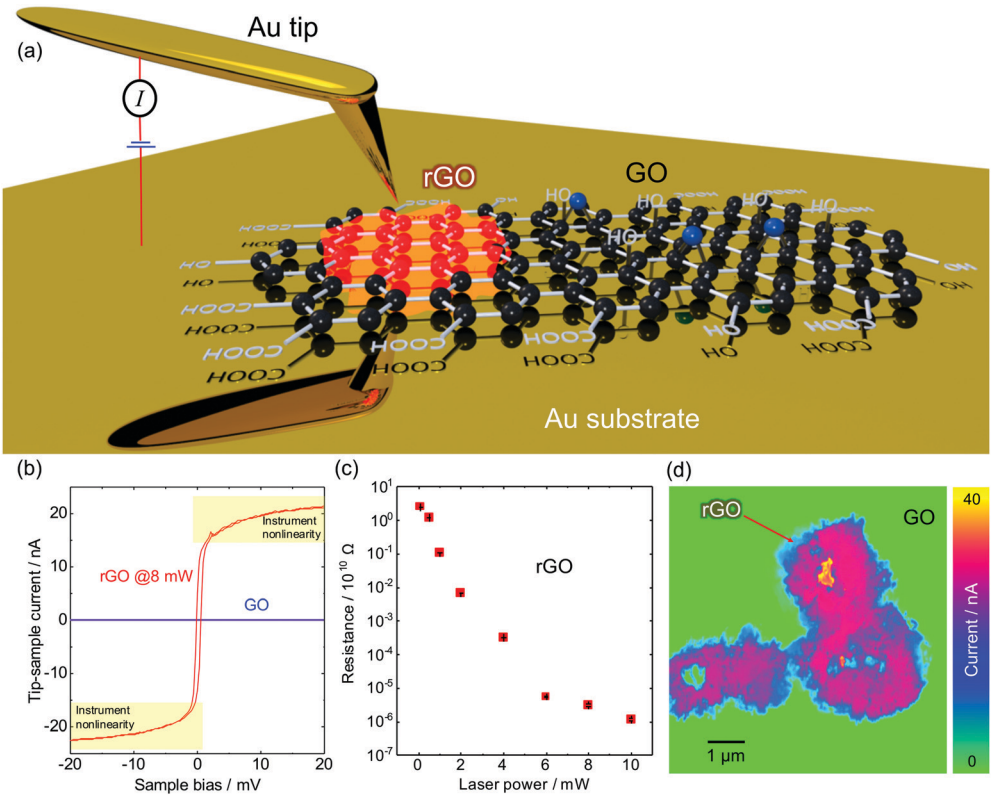

Fig. 2 (a) Schematic (non-scaled) representation of the CSAFM experiment. (b) CSAFM *I*–*V* curves of rGO reduced with 8 mW power. (c) The resistance of rGOs *vs.* laser power. (d) CSAFM current image obtained under a tip-sample bias of 500 mV on a rGO spot reduced with a laser power of 8 mW.

cylindrical conductor of 50 nm radius given by the tip size. The height of the cylinder corresponds to the GO thickness of about 103 nm (we do not consider the decrease in the film thickness after reduction which could result in an overestimation of conductivity). These dimensions, summarized in the inset of Fig. S3b (ESI†), result in an estimation of the rGO conductivity of 433 S m^{-1}. This conductivity value is in close agreement with the conductivity of graphite 330 S m^{-1} determined perpendicular to the basal plane.[28] We must recognize that our conductivity estimation for rGO is based on considering a uniform conductive medium thus neglecting any anisotropy in the film. This is not justified given the high anisotropy of rGO. However, the correct way to calculate the conductivity implies writing it as a rank-2 tensor to take into account the anisotropy which requires a much deeper and detailed analysis of the internal structure of rGO films which is beyond the scope of this work. Keeping these points in mind, we focus herein on the resistance directly determined from the *IV* curves. We observe that at the beginning of annealing, the rGO resistance decreases rapidly. The reason is that large amounts of hydroxyl groups are removed by laser annealing at low laser power and as a result, the sp^2 carbon content ratio in the GO sheet drastically increases. This interpretation is based on previous molecular dynamics results showing that hydroxyl groups are the ones that require the least energy for removal in the thermal reduction of GO, also leaving the sp^2 lattice intact.[29] Additionally, the distance between rGO sheets becomes shorter lowering the barrier for electron transport which contributes to the decrease in the resistance.[27]

We observed the lowest resistance of about 10 kΩ for the sample obtained under 10 mW laser power irradiation. Fig. 2d shows a CSAFM current image for rGO reduced by a power of 8 mW using 0.5 V bias voltage where we can clearly distinguish the GO and rGO regions. The green region in Fig. 2d corresponds to GO since there is no current in this region. The width of the reduced region is 1.3 μm or less. We could control the laser irradiation parameters such as the objective numerical aperture or the laser wavelength to decrease the rGO spot size. What is more technologically interesting, and also as reported in previous works,[16,30] is the possibility to easily control the shape of the reduced region by controlling the laser location to obtain arbitrary patterns. It is also worth noting that there are no apparent topographical changes in the microstructure of the laser-illuminated spot as reflected in the AFM image in Fig. S3 (ESI†), the calculated RMS roughness is *ca.* 9 nm. The thickness of the GO film is about 103 nm which also corresponds to the depth of the laser reduction; otherwise, we would not get any current flow through the rGO films. More details are shown in Fig. S4 (ESI†).

Raman spectra

We obtained the Raman spectra for the same laser-irradiated rGO samples discussed above in the electrical investigation. The spectra were obtained with a high magnification 100× objective

that allowed us to focus the laser spot on the laser-reduced regions as shown in Fig. S1b (ESI†). The Raman spectroscopy results are shown in Fig. 3a. The spectra display the carbon D and G bands centered at ~1350 and ~1580 cm^{-1}, respectively. The G band (~1583 cm^{-1}) is related to the first-order E_{2g} optical mode of graphite and the in-plane stretching of the C=C bonds.[31,32] The D band (~1350 cm^{-1}) is assigned to an A_{1g} breathing mode at the Brillouin zone boundary K. Its intensity is associated with the number of defects in the graphene plane.[33] The D′ band (~1620 cm^{-1}) corresponds to the intravalley double-resonance process that becomes Raman active in the presence of defects.[34] The effects of reduction in the Raman spectra were already observed in one of the pioneer works on the applications of laser-reduced GO.[30] In particular, Zhang *et al.* reported the decrease in D and G peak widths and the increase of the D/G intensity ratio for the femtosecond laser reduction of GO.

The second-order bands are observed in the range from 2500 to 3200 cm^{-1}. The 2D band centered at 2700 cm^{-1} (also called the G′ band), is the overtone of the D band activated by a double-resonance process similar to the D band, but requiring scattering of two phonons with opposite wave vectors to ensure momentum conservation and its activation.[24,35] It is called the 2D band because it involves two of the same phonons responsible for the D band. But in contrast to the D band, the 2D does not require the presence of defects to fulfill the momentum conservation law, and thus it is always visible in the second-order Raman spectra of graphene (or any other sp^2 carbon).[36] The 2G (~3170 cm^{-1}) band is attributed to the overtone of the G band, and the D + G band (~2940 cm^{-1}) is the combined overtone of the D and G band.[24,35] In some reports, the D + G band was also assigned to the D + D′, and the 2G band was assigned to the 2D′ or also to the G + D′.[37,38] But according to Malard's *et al.* report, the D + G (~2940 cm^{-1}) with D + D′ (~2970 cm^{-1}) band and 2G (~3170 cm^{-1}) with 2D′ or G + D′ (~3205 cm^{-1}) band were assigned totally differently.[39] In their report, the ~2970 cm^{-1} mode was attributed to the combination of D and D′ bands (D + D′), while the 3205 cm^{-1} was assigned to the combination of G and D′ bands (G + D′). It is important to keep in mind these contradictions in the analysis of the second-order modes.

Fig. 3b shows an example of numerical fitting for the Raman spectrum of the rGO laser-annealed at 0.1 mW. The rest of the fitted spectra are shown in the ESI† (Fig. S5). In Fig. 3b, we found that the spectra could be fitted with 6 + 3 = 9 peaks for the first and second order regions. In addition to the well-known D and G bands, there are several other peaks labeled D*, D″, and D′ in the range from 1000 to 1800 cm^{-1} which have been reported in recent works.[21,37] In those works, it was observed that as the oxygen content of rGO increased the band position of D* decreased while the position of D″ went up. Our observations agree with their work in using those peaks to fit the spectra properly but unfortunately, or rather interestingly, we did not find the same correlation regarding the change in the peak position and the degree of reduction. Partly, this is because the D* and D″ are broad bands located close to the D and G peaks. Moreover, despite recent calculations that assigned the D″ peak to the presence of oxygen,[40] the peak positions can only be fitted with high uncertainty resulting in the low precision of the fitting method. The issues with the D* and D″ fitting could be a consequence of the different reduction processes used in our work and that used in the previous Raman spectroscopy report.[21] We also detected the M peak of graphite centered at 1730 cm^{-1} which was not considered in previous works most likely due to its low intensity. This peak is attributed to an intravalley resonant scattering process originating from the combination mode of the out-of-plane layer-breathing mode and the in-plane longitudinal optical mode.[41,42] However, in our work, the M band was too weak to take its fitting parameters into account. Moreover, here, we are more interested in the second-order and combination of 2D, D + G, 2G modes in the range from 2500 to 3200 cm^{-1}. We performed a fit analysis of these peaks with Lorentzian functions. The 2G (~3170 cm^{-1}) band was attributed to the overtone of the G band, and the D + G band (~2940 cm^{-1}) is the combined overtone of the D and G band.[24,35] Since the D, 2D, D + G,

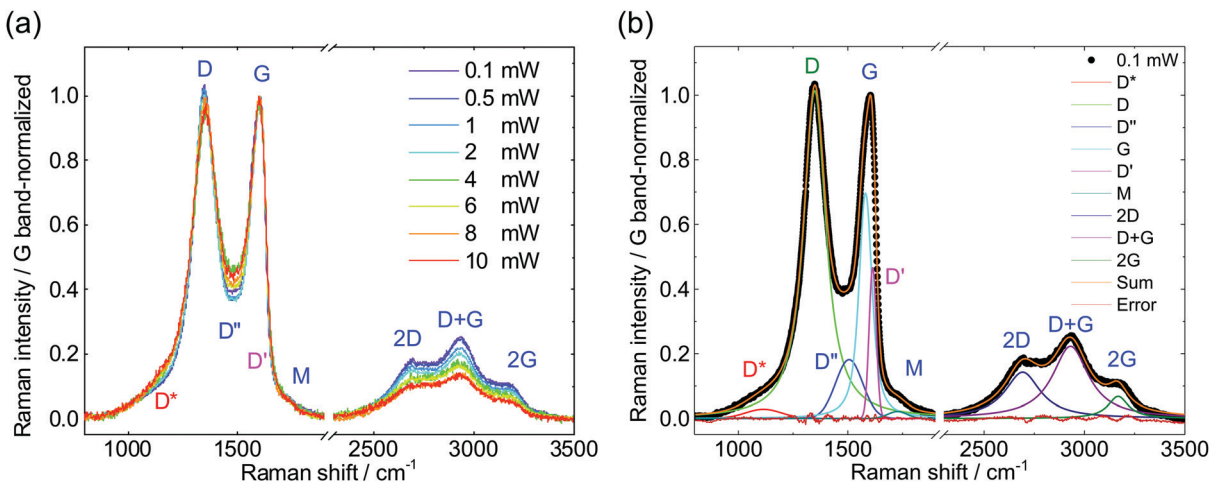

Fig. 3 (a) Raman spectra of rGOs reduced by laser annealing with different powers (ranging from 0.1 mW to 10 mW). (b) An example of the Raman spectrum fitting for rGO reduced by laser with a power of 0.1 mW.

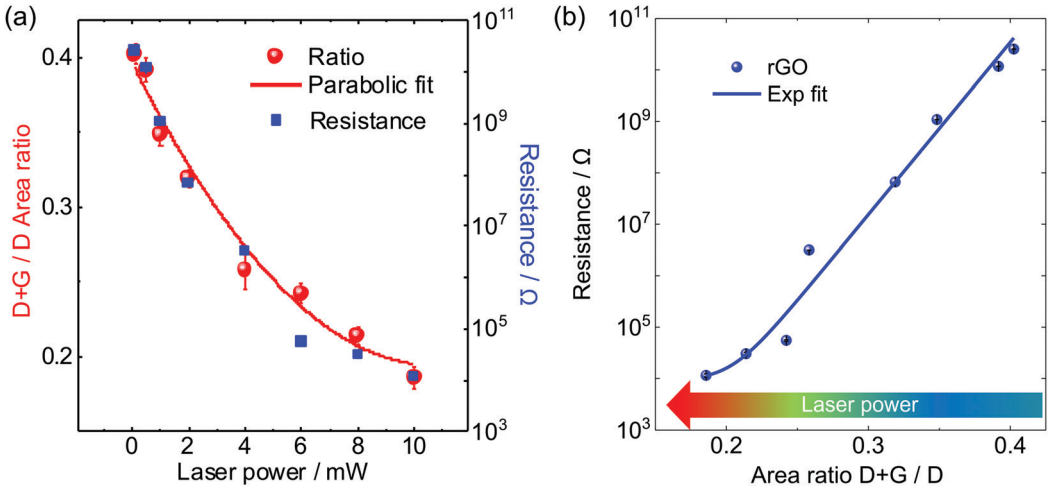

Fig. 4 (a) Area ratio of A_{D+G}/A_D (left side, red scale) and resistance (right side, blue scale) of rGO *vs.* laser power, the parabolic fit is only for the area ratio A_{D+G}/A_D. (b) Plot for the electrical resistance of rGO against the A_{D+G}/A_D area ratio. The numerical fit is only an empirical guide to the eye.

and 2G bands can be fitted without significant overlap with other bands, we expected that the spectral parameters of these bands are more reliable to correlate with the changes in laser-reduced graphene oxide. As an example, consider the A_{D+G}/A_D area ratio and the electrical resistance of rGO as a function of laser power as shown in Fig. 4 in which a clear correlation between spectral and electrical parameters is observed. This correlation was not reported before.

The parabolic function used to fit the area ratio A_r as a function of laser power L_{pw} shown in Fig. 4a (and Fig. 5a below) is $A_r = 0.4 - 0.04L_{pw} + 1.8 \times 10^{-3}L_{pw}^2$. The correlation between area ratio and laser power and the rGO resistance *vs.* area ratio are plotted in Fig. 5. In Fig. 5a and b, we see that all the area ratios A_{D+G}/A_D, A_{2G}/A_D, and A_{2G}/A_{D+G} decrease as the laser-reduction power increases, and also the degree of reduction increases. These area ratio parameters show the same dependence as the electrical resistance on the laser power used for reduction.

The D band depends on the defects around sp^2 carbon atoms in graphitic materials. By increasing the defect concentration, the D peak intensity increases, but it does not increase indefinitely. As the defect density increases the D band intensity reaches a maximum as shown in Fig. S6 (ESI†). By further increasing the defect density, the D band intensity starts to decrease because the graphene sheet becomes dominated by the structurally-disordered areas as previously reported by M. M. Lucchese *et al.*[33,43] In their work, they used Ar^+ ion bombardment to increase the defect density in graphene obtaining spectra that match closely the spectra of GO and rGO. Similarly, in GO a large number of defects is caused by oxygen-containing groups. Moreover, in our case, the laser annealing can induce some new defects in GO during the desorption of epoxy groups by forming CO_2 and CO gases.[9] The D bandwidth was proposed as a good indicator of the degree of reduction.[27] We found a linear change in the D bandwidth with the laser power at a rate

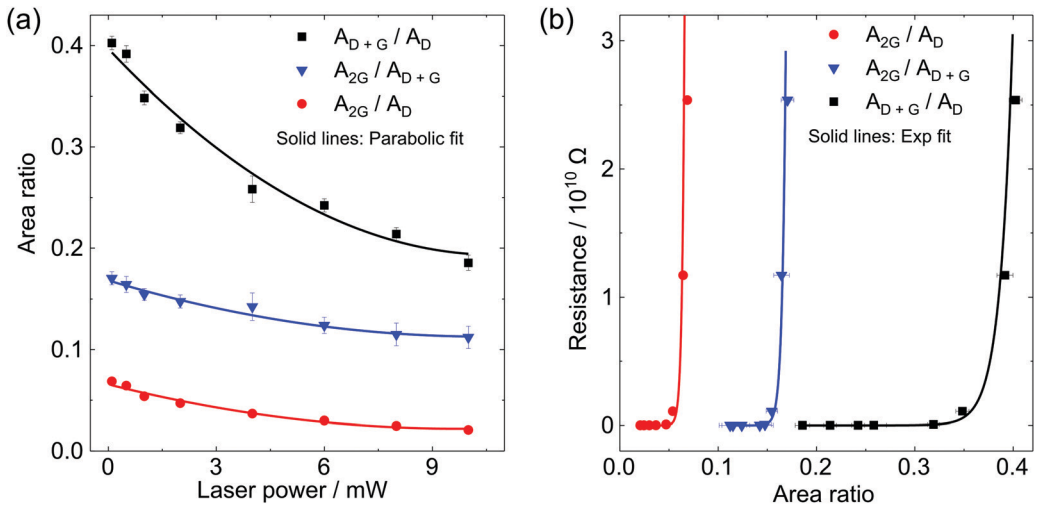

Fig. 5 (a) Area ratio of A_{D+G}/A_D, A_{2G}/A_D and A_{2G}/A_{D+G} change with laser power. The curves were fitted using a second-order function. (b) Area ratio of A_{D+G}/A_D, A_{2G}/A_D and A_{2G}/A_{D+G} change with resistance.

of (4.1 ± 0.2) cm^{-1} mW^{-1} within the range of 140 to 180 cm^{-1}, see Fig. S7a (ESI†). According to previous observations,[27] the range of D width change we observe in our work should correspond to a non-monotonic dependence with annealing temperature representing an sp^2 content below 70%. Therefore, the D bandwidth is not that useful in our case since it does not correlate with the nonlinear changes in the electrical properties, but it shows a linear behavior with laser annealing in contrast to ref. 27. This discrepancy could reflect the differences between the thermal and laser reduction of GO.

For the bands 2D, D + G, and 2G in the range from 2500 to 3200 cm^{-1}, we observe an intensity lowering trend as the laser power increases, see Fig. 3a. The 2D band originates from a double-resonance effect involving a two-phonon scattering process. Therefore, with an increase in the number of defects in graphene, one of the two inelastic phonon scattering processes of 2D is affected resulting in a decrease in that mode. As we discussed before, the laser annealing of GO may induce some new defects, and this can be viewed as a conversion of the 2D to D band.[44] Similarly, the other overtone bands D + G and 2G decreased with increasing laser power. The 2D, D + G, and 2G are highly structure-sensitive. It was reported by Karthikeyan Krishnamoorthy *et al.* that the changes in overtone bands (2D, D + G, and 2G bands) illustrate the disruption of the graphitic AB stacking order in GO with increasing oxidation level.[35] Especially for D + G which was caused by lattice disorder.[45] Hence, in the process of removing epoxy groups, the laser annealing also induces defects. Those defects make the D peak width larger and at the same time decrease the intensity of higher order modes. As a consequence, the area ratios A_{D+G}/A_D, A_{2G}/A_D and A_{2G}/A_{D+G} decrease when the annealing laser power increases and is the same as the decrease of resistance of rGO. It is also worth noting that although for laser-induced rGO our analysis using the second-order modes is reported now for the first time, and Vollebregt and collaborators demonstrated the use of the second-order modes in the Raman spectra of carbon fibers and nanotubes as a measure of sample quality.[24] Also, Trusovas and collaborators showed a decrease in the 2D peak width with the increase in the laser power.[46] Our work emphasizes the usefulness of minding these second-order modes in the analysis of laser-induced rGO that until now were mostly neglected.

Discussion of the Raman and electrical characterization results

Upon increasing the laser power, the electrical resistance drastically drops due to the relatively gentle removal of hydroxyl groups. The hydroxyls can be easily removed without significantly inducing defects as shown in a previous report.[29] At higher laser power, the decrease in the resistance reaches a plateau in the linear scale plot; this can be seen in Fig. S2 (ESI†). The reason for this plateau is that the further reduction of GO continues now by the removal of the remaining oxygen-containing groups such as carboxyl and epoxy. These latter groups require more energy resulting in CO and CO_2 gas release and the creation of new structural defects in rGO.[46] The decrease in the second-order mode areas further points to partial carbon amorphization.[32] Although the D/G ratio decreases, as an indication of a larger degree of reduction (more sp^2 carbon), the increase of the D peak width and the decrease of intensity ratios shown in Fig. S7 (ESI†) can also be understood as due to the formation of sp^2 clusters surrounded by an amorphous phase. Moreover, this amorphous phase acts as charge traps. This hypothesis was supported by Kelvin probe force microscopy investigations of a crystalline graphite sample that had localized defects made by a focused ion beam (these results are being published elsewhere). This scenario explains why the D/G ratio decreases even though the structural defects increase at high laser power since charged impurity defects do not activate the D band.[47,48] Therefore we have two possible but not mutually exclusive effects with opposite contributions to the Raman spectra and the electrical conductivity of laser-reduced GO. On one side we have the reduction, the conversion of sp^3 carbon to sp^2; on the other hand, we have the structural defects induced by the gas release at high laser power. The electrical conductivity is affected the most because the defects at high laser power decrease the mobility of electrons made available after reduction. This can be understood since the electrical conductivity is directly proportional to the charge carrier density, charge carrier mobility, and the electric field. The electric field is constant and externally controlled by the bias potential on the sample. Therefore, if the rate of conductivity *vs.* laser power changes, it implies the charge carrier density and/or mobility change. We expect the charge carrier to increase due to the formation of more sp^2 carbon as the laser power increases. But at the same time, the structural defects decrease the charge carrier mobility. The mobility reduction may also be linked to the charge traps which do not activate the D band but decrease the intensity of the second-order modes (like the 2D band).[47] The fact that we still see a continuous decrease in the resistivity as the laser power increases indicates that the generation of free charge carriers compensates the carrier mobility reduction. Note from Fig. S7b (ESI†) that the D/G intensity ratio decreases as the laser power increases which could imply, as mentioned above, that we are in a highly defective regime as exemplified by Fig. S6 (ESI†). Ideally, we should be able to distinguish between these two mechanisms that affect the D/G intensity ratio: (1) generation of charged impurities that do not activate the D band, or (2) the presence and further generation of highly defective sp^2 carbon. This latter interpretation is in agreement with the plasma-induced oxidation of graphene, particularly in the highly-defective regime, in the transition from stage 1 to stage 2.[49] However, it was only reported that the area changes for the 2D but not for the other higher order modes reported in this work. Note that the complementary spectroscopic methods such as IR absorption cannot be easily applied to this kind of sample due to the small spatial dimensions. Therefore, additional nanoscale studies involving complementary Kelvin probe force microscopy imaging, confocal Raman spectroscopy, and tip-enhanced Raman spectroscopy (TERS)[50] of laser-reduced graphene oxide are underway to answer this and other open questions that still elude us.

Conclusions

We investigated graphene oxide films reduced by laser annealing with different laser powers. We aimed to identify a link between the degree of reduction reflected by the electrical conductivity and the peak characteristics in the Raman spectra. We obtained the rGO conductivity from *I–V* curves at the nanoscale using conductive atomic force microscopy (CSAFM) of exactly the same samples analyzed by Raman spectroscopy. CSAFM results allowed us to correlate the resistance of rGO with the degree of reduction. The current image of rGO revealed the size of the reduced regions which is in the order of the laser spot size *ca.* 1.3 μm. In agreement with the expectations from thermal annealing reduction reported at the macroscale,[51] we found that the resistance of rGO decreased as the laser power increased due to the thermal energy provided by the electromagnetic field. However, previous analysis based on rGO obtained by thermal reduction did not apply to the laser-reduced GO. This discrepancy could be due to the photochemical contribution to GO reduction that is absent in thermally annealed samples. The dependence of electrical resistance on laser power is highly non-linear and changes drastically for a laser power in the range 0.1–4 mW, and then slows down for a laser power larger than 4 mW. We attribute this result to the degree of reduction that reaches a saturation point after a significant amount of hydrogen and oxygen-containing groups (hydroxyls) are eliminated. The Raman spectra of rGO were deconvoluted and fitted by several peaks including D*, D, D″, G, D′, M, 2D, D + G, 2G bands. Among all these Raman modes, we found that only the D, 2D, D + G, and 2G bands could be reliably fitted. We exploited this robust fitting analysis to establish a correlation with the laser power and electrical conductivity. This correlation that was not reported before is given by the area ratios between the first and second order regions A_{D+G}/A_D, A_{2G}/A_D, and A_{2G}/A_{D+G}, the lower these ratios, the higher the degree of reduction. We attribute the correlation of the 2D, D + G, and 2G bands to the high sensitivity of these modes to the electronic structure perturbations of sp^2 carbons, especially the D + G band which is caused by lattice disorder. The findings in our investigation provide a new and alternative Raman spectroscopy analysis method for laser-reduced graphene oxide that allows linking the degree of reduction and the electrical conductivity. By performing a simple optical spectroscopy measurement, we can now evaluate the electrical conductivity of a set of rGO samples even without the need of making electrical contacts. These results are of significance to the community working on graphene-oxide materials allowing conductivity and structural studies of rGO-based microdevices with a high spatial resolution (∼μm).

Conflicts of interest

The authors declare no conflict.

Acknowledgements

We are very grateful to Olga Nozdrina from TPU for help in initiating the laser-induced research at Tomsk, and to Alexey Yakovlev, Elena Polysadova, and Mekhman Yusubov for their essential support that made this research possible. We are thankful to Ammar Al-Hamry, Varnika Prakash, and Olfa Kanoun for providing the GO material and for fruitful discussions. This research was supported by the Tomsk Polytechnic University Competitiveness Enhancement Program 5-100.

References

1 M. J. Allen, V. C. Tung and R. B. Kaner, Honeycomb carbon: a review of graphene, *Chem. Rev.*, 2010, **110**, 132–145.
2 K. S. Novoselov, A. K. Geim, S. V. Morozov, D. Jiang, Y. Zhang, S. V. Dubonos, I. V. Grigorieva and A. A. Firsov, Electric field effect in atomically thin carbon films, *Science*, 2004, **306**, 666–669.
3 I. W. Frank, D. M. Tanenbaum, A. M. van der Zande and P. L. McEuen, Mechanical properties of suspended graphene sheets, *J. Vac. Sci. Technol., B: Microelectron. Nanometer. Struct.–Process., Meas., Phenom.*, 2007, **25**, 2558–2561.
4 A. H. C. Neto, A. H. Castro Neto, F. Guinea, N. M. R. Peres, K. S. Novoselov and A. K. Geim, *Rev. Mod. Phys.*, 2009, **81**, 109.
5 R. R. Nair, P. Blake, A. N. Grigorenko, K. S. Novoselov, T. J. Booth, T. Stauber, N. M. R. Peres and A. K. Geim, Fine structure constant defines visual transparency of graphene, *Science*, 2008, **320**, 1308.
6 H. Jang, Y. J. Park, X. Chen, T. Das, M.-S. Kim and J.-H. Ahn, Graphene-Based Flexible and Stretchable Electronics, *Adv. Mater.*, 2016, **28**, 4184–4202.
7 P. T. Yin, T.-H. Kim, J.-W. Choi and K.-B. Lee, Prospects for graphene-nanoparticle-based hybrid sensors, *Phys. Chem. Chem. Phys.*, 2013, **15**, 12785–12799.
8 K. P. Loh, Q. Bao, G. Eda and M. Chhowalla, Graphene oxide as a chemically tunable platform for optical applications, *Nat. Chem.*, 2010, **2**, 1015–1024.
9 S. Pei and H.-M. Cheng, The reduction of graphene oxide, *Carbon N. Y.*, 2012, **50**, 3210–3228.
10 B. Martín-García, M. M. Velázquez, F. Rossella, V. Bellani, E. Diez, J. L. García Fierro, J. A. Pérez-Hernández, J. Hernández-Toro, S. Claramunt and A. Cirera, Functionalization of reduced graphite oxide sheets with a zwitterionic surfactant, *ChemPhysChem*, 2012, **13**, 3682–3690.
11 C. K. Chua and M. Pumera, Chemical reduction of graphene oxide: a synthetic chemistry viewpoint, *Chem. Soc. Rev.*, 2014, **43**, 291–312.
12 H. C. Schniepp, J.-L. Li, M. J. McAllister, H. Sai, M. Herrera-Alonso, D. H. Adamson, R. K. Prud'homme, R. Car, D. A. Saville and I. A. Aksay, Functionalized single graphene sheets derived from splitting graphite oxide, *J. Phys. Chem. B*, 2006, **110**, 8535–8539.
13 K. N. Kudin, B. Ozbas, H. C. Schniepp, R. K. Prud'homme, I. A. Aksay and R. Car, Raman spectra of graphite oxide and functionalized graphene sheets, *Nano Lett.*, 2008, **8**, 36–41.
14 A. Al-Hamry, H. Kang, E. Sowade, V. Dzhagan, R. D. Rodriguez, C. Müller, D. R. T. Zahn, R. R. Baumann and O. Kanoun, Tuning the reduction and conductivity of solution-processed

graphene oxide by intense pulsed light, *Carbon N. Y.*, 2016, **102**, 236–244.

15 R. Trusovas, G. Račiukaitis, G. Niaura, J. Barkauskas, G. Valušis and R. Pauliukaite, Recent Advances in Laser Utilization in the Chemical Modification of Graphene Oxide and Its Applications, *Adv. Opt. Mater.*, 2016, **4**, 37–65.

16 W. Gao, N. Singh, L. Song, Z. Liu, A. L. M. Reddy, L. Ci, R. Vajtai, Q. Zhang, B. Wei and P. M. Ajayan, Direct laser writing of micro-supercapacitors on hydrated graphite oxide films, *Nat. Nanotechnol.*, 2011, **6**, 496–500.

17 Y.-L. Zhang, L. Guo, H. Xia, Q.-D. Chen, J. Feng and H.-B. Sun, Photoreduction of Graphene Oxides: Methods, Properties, and Applications, *Adv. Opt. Mater.*, 2014, **2**, 10–28.

18 M. S. Dresselhaus, A. Jorio, M. Hofmann, G. Dresselhaus and R. Saito, Perspectives on carbon nanotubes and graphene Raman spectroscopy, *Nano Lett.*, 2010, **10**, 751–758.

19 A. Jorio and L. G. Cançado, Perspectives on Raman spectroscopy of graphene-based systems: from the perfect two-dimensional surface to charcoal, *Phys. Chem. Chem. Phys.*, 2012, **14**, 15246–15256.

20 A. C. Ferrari, Raman spectroscopy of graphene and graphite: disorder, electron–phonon coupling, doping and nonadiabatic effects, *Solid State Commun.*, 2007, **143**, 47–57.

21 S. Claramunt, A. Varea, D. López-Díaz, M. M. Velázquez, A. Cornet and A. Cirera, The Importance of Interbands on the Interpretation of the Raman Spectrum of Graphene Oxide, *J. Phys. Chem. C*, 2015, **119**, 10123–10129.

22 A. Sadezky, H. Muckenhuber, H. Grothe, R. Niessner and U. Pöschl, Raman microspectroscopy of soot and related carbonaceous materials: spectral analysis and structural information, *Carbon N. Y.*, 2005, **43**, 1731–1742.

23 R. J. Nemanich and S. A. Solin, First- and second-order Raman scattering from finite-size crystals of graphite, *Phys. Rev. B: Condens. Matter Mater. Phys.*, 1979, **20**, 392–401.

24 S. Vollebregt, R. Ishihara, F. D. Tichelaar, Y. Hou and C. I. M. Beenakker, Influence of the growth temperature on the first and second-order Raman band ratios and widths of carbon nanotubes and fibers, *Carbon N. Y.*, 2012, **50**, 3542–3554.

25 W. Chen, L. Yan and P. R. Bangal, Preparation of graphene by the rapid and mild thermal reduction of graphene oxide induced by microwaves, *Carbon N. Y.*, 2010, **48**, 1146–1152.

26 P. Kumar, K. S. Subrahmanyam and C. N. R. Rao, Graphene Produced by Radiation-Induced Reduction of Graphene Oxide, *Int. J. Nanosci.*, 2011, **10**, 559–566.

27 X. Díez-Betriu, S. Álvarez-García, C. Botas, P. Álvarez, J. Sánchez-Marcos, C. Prieto, R. Menéndez and A. de Andrés, Raman spectroscopy for the study of reduction mechanisms and optimization of conductivity in graphene oxide thin films, *J. Mater. Chem.*, 2013, **1**, 6905–6912.

28 H. O. Pierson, *Handbook of Carbon, Graphite, Diamonds and Fullerenes: Processing, Properties and Applications*, William Andrew, 2012.

29 A. Bagri, C. Mattevi, M. Acik, Y. J. Chabal, M. Chhowalla and V. B. Shenoy, Structural evolution during the reduction of chemically derived graphene oxide, *Nat. Chem.*, 2010, **2**, 581–587.

30 Y. Zhang, L. Guo, S. Wei, Y. He, H. Xia, Q. Chen, H.-B. Sun and F.-S. Xiao, Direct imprinting of microcircuits on graphene oxides film by femtosecond laser reduction, *Nano Today*, 2010, **5**, 15–20.

31 S. Reich and C. Thomsen, Raman spectroscopy of graphite, *Philos. Trans. R. Soc., A*, 2004, **362**, 2271–2288.

32 E. H. Martins Ferreira, M. V. O. Moutinho, F. Stavale, M. M. Lucchese, R. B. Capaz, C. A. Achete and A. Jorio, Evolution of the Raman spectra from single-, few-, and many-layer graphene with increasing disorder, *Phys. Rev. B: Condens. Matter Mater. Phys.*, 2010, **82**, 125429.

33 L. G. Cançado, A. Jorio, E. H. M. Ferreira, F. Stavale, C. A. Achete, R. B. Capaz, M. V. O. Moutinho, A. Lombardo, T. S. Kulmala and A. C. Ferrari, Quantifying defects in graphene via Raman spectroscopy at different excitation energies, *Nano Lett.*, 2011, **11**, 3190–3196.

34 D. C. Elias, R. R. Nair, T. M. G. Mohiuddin, S. V. Morozov, P. Blake, M. P. Halsall, A. C. Ferrari, D. W. Boukhvalov, M. I. Katsnelson, A. K. Geim and K. S. Novoselov, Control of graphene's properties by reversible hydrogenation: evidence for graphane, *Science*, 2009, **323**, 610–613.

35 K. Krishnamoorthy, M. Veerapandian, K. Yun and S.-J. Kim, The chemical and structural analysis of graphene oxide with different degrees of oxidation, *Carbon N. Y.*, 2013, **53**, 38–49.

36 A. C. Ferrari, J. C. Meyer, V. Scardaci, C. Casiraghi, M. Lazzeri, F. Mauri, S. Piscanec, D. Jiang, K. S. Novoselov, S. Roth and A. K. Geim, Raman spectrum of graphene and graphene layers, *Phys. Rev. Lett.*, 2006, **97**, 187401.

37 D. López-Díaz, M. López Holgado, J. L. García-Fierro and M. M. Velázquez, Evolution of the Raman Spectrum with the Chemical Composition of Graphene Oxide, *J. Phys. Chem. C*, 2017, **121**, 20489–20497.

38 A. Kaniyoor and S. Ramaprabhu, A Raman spectroscopic investigation of graphite oxide derived graphene, *AIP Adv.*, 2012, **2**, 032183.

39 L. M. Malard, M. A. Pimenta, G. Dresselhaus and M. S. Dresselhaus, Raman spectroscopy in graphene, *Phys. Rep.*, 2009, **473**, 51–87.

40 P. Vecera, J. C. Chacón-Torres, T. Pichler, S. Reich, H. R. Soni, A. Görling, K. Edelthalhammer, H. Peterlik, F. Hauke and A. Hirsch, Precise determination of graphene functionalization by in situ Raman spectroscopy, *Nat. Commun.*, 2017, **8**, 15192.

41 C. H. Lui, L. M. Malard, S. Kim, G. Lantz, F. E. Laverge, R. Saito and T. F. Heinz, Observation of layer-breathing mode vibrations in few-layer graphene through combination Raman scattering, *Nano Lett.*, 2012, **12**, 5539–5544.

42 A. Jorio, R. Saito, G. Dresselhaus and M. S. Dresselhaus, *Raman Spectroscopy in Graphene Related Systems*, Wiley-VCH Verlag GmbH & Co. KGaA, Weinheim, Germany, 2011.

43 M. M. Lucchese, F. Stavale, E. H. M. Ferreira, C. Vilani, M. V. O. Moutinho, R. B. Capaz, C. A. Achete and A. Jorio, Quantifying ion-induced defects and Raman relaxation length in graphene, *Carbon N. Y.*, 2010, **48**, 1592–1597.

44 B. Krauss, T. Lohmann, D.-H. Chae, M. Haluska, K. von Klitzing and J. H. Smet, Laser-induced disassembly of a graphene single crystal into a nanocrystalline network, *Phys. Rev. B: Condens. Matter Mater. Phys.*, 2009, **79**, 165428.
45 T. C. Chieu, M. S. Dresselhaus and M. Endo, Raman studies of benzene-derived graphite fibers, *Phys. Rev. B: Condens. Matter Mater. Phys.*, 1982, **26**, 5867–5877.
46 R. Trusovas, K. Ratautas, G. Račiukaitis, J. Barkauskas, I. Stankevičienė, G. Niaura and R. Mažeikienė, Reduction of graphite oxide to graphene with laser irradiation, *Carbon N. Y.*, 2013, **52**, 574–582.
47 C. Casiraghi, S. Pisana, K. S. Novoselov, A. K. Geim and A. C. Ferrari, Raman fingerprint of charged impurities in graphene, *Appl. Phys. Lett.*, 2007, **91**, 233108.
48 M. Bruna, A. K. Ott, M. Ijäs, D. Yoon, U. Sassi and A. C. Ferrari, Doping dependence of the Raman spectrum of defected graphene, *ACS Nano*, 2014, **8**, 7432–7441.
49 A. Eckmann, A. Felten, A. Mishchenko, L. Britnell, R. Krupke, K. S. Novoselov and C. Casiraghi, Probing the nature of defects in graphene by Raman spectroscopy, *Nano Lett.*, 2012, **12**, 3925–3930.
50 E. Sheremet, R. D. Rodriguez, A. L. Agapov, A. P. Sokolov, M. Hietschold and D. R. T. Zahn, Nanoscale imaging and identification of a four-component carbon sample, *Carbon N. Y.*, 2016, **96**, 588–593.
51 N.-J. Song, C.-M. Chen, C. Lu, Z. Liu, Q.-Q. Kong and R. Cai, Thermally reduced graphene oxide films as flexible lateral heat spreaders, *J. Mater. Chem. A*, 2014, **2**, 16563–16568.

